



HAL
open science

Support vectors machines regression for estimation of Mars surface physical properties

Caroline Bernard-Michel, Sylvain Douté, Mathieu Fauvel, Laurent Gardes,
Stéphane Girard

► **To cite this version:**

Caroline Bernard-Michel, Sylvain Douté, Mathieu Fauvel, Laurent Gardes, Stéphane Girard. Support vectors machines regression for estimation of Mars surface physical properties. ESANN 2009 - 17th European Symposium on Artificial Neural Networks, Apr 2009, Bruges, Belgium. pp.195-200. hal-00761724v1

HAL Id: hal-00761724

<https://hal.science/hal-00761724v1>

Submitted on 7 Dec 2012 (v1), last revised 6 May 2014 (v2)

HAL is a multi-disciplinary open access archive for the deposit and dissemination of scientific research documents, whether they are published or not. The documents may come from teaching and research institutions in France or abroad, or from public or private research centers.

L'archive ouverte pluridisciplinaire **HAL**, est destinée au dépôt et à la diffusion de documents scientifiques de niveau recherche, publiés ou non, émanant des établissements d'enseignement et de recherche français ou étrangers, des laboratoires publics ou privés.

Support Vectors Machines Regression for Estimation of Mars Surface Physical Properties

C. Bernard-Michel¹, S. Douté², M. Fauvel¹, L. Gardes¹, and S. Girard¹ *

1- MISTIS, INRIA Rhône-Alpes & Laboratoire Jean Kuntzmann, Grenoble, France

2- Laboratoire de Planétologie de Grenoble, Grenoble, France

Abstract. In this paper, the estimation of physical properties from hyperspectral data with support vector machine is addressed. Several kernel functions were used, from classical to advanced ones. The results are compared with Gaussian Regularized Sliced Inversion Regression and Partial Least Squares, both in terms of accuracy and complexity. Experiments on simulated data show that SVM produce highly accurate results, for some kernels, but with an increased of the processing time. Inversion of real images shows that SVM are robust and generalize well. In addition, the analysis of the support vectors allows to detect saturation of the physical model used to generate the simulated data.

1 Introduction

Hyperspectral images are now a key tool for the analysis of remote planets [1, 2]. The very high resolution in the spectral domain allows a fine characterization of the physical properties of the scene. For instance, the OMEGA sensor acquires the spectral radiance coming from the planet in more than 200 contiguous spectral channels. Each pixel of the image is represented by a spectra/vector $\mathbf{x} \in \mathbb{R}^d$ for which each component corresponds to a particular wavelength, d being the total number of wavelengths. Chemical composition, granularity, texture, and physical state are some of the parameters that characterize the morphology of spectra and thus of the area of interest.

Deducing the physical parameters \mathbf{y} from the observed spectra \mathbf{x} is a central problem in classical physics, called an *inverse problem*. Since it generally cannot be solved analytically, the use of optimization or statistical methods is necessary. Solving inverse problems requires an adequate understanding of the fundamental physics, *i.e.* a functional relation between \mathbf{x} and \mathbf{y} must be specified: $\mathbf{x} = g(\mathbf{y})$. Given g , different methods can be used to deduce the parameter from new observations. Current solutions to the inverse problem can be divided into three main categories (for further details and comparisons, see [3]):

1. *Optimization algorithms*: These methods minimize an objective quality function that measures the fit between \mathbf{x} and $g(\mathbf{y})$. Inverse problems are often ill-posed, therefore estimation can be unstable and regularization is needed. For instance, a prior distribution on model parameter can be used.

*This work is supported by a contract with CNES through its Groupe Système Solaire Program and by INRIA and with the financial support of the "Agence Nationale de la Recherche" (French Research Agency) through its MDCO program ("Masse de Données et COonnaissances"). The Vahiné project was selected in 2007 under the reference ANR-07-MDCO-013.

2. *Look-Up Table (LUT) / k-nearest neighbors approach (k-nn)*: A large database (LUT) is generated by radiative transfer for many parameter values. Each observed spectrum is then compared with the LUT spectra in order to find the best match (the nearest neighbor), according to an objective function minimization. Parameters are then deduced from this best match.
3. *Training approaches*: A functional relation $\mathbf{y} = f(\mathbf{x})$ between spectra and parameters is assumed, such as $f^{-1} = g$, and a LUT is used to estimate f . For instance Training approaches include neural network approaches.

Hyperspectral images must be inverted with the following constraints: *a)* Large data-sets and various models require fast methodologies, *b)* High-dimensional data and “curse of dimensionality” with the associated sparsity issues require simple model with few parameters, *c)* Noisy spectra must be accounted for. Optimization based approaches suffer from heavy computational load and thus are not adapted to hyperspectral images. Nearest neighbors algorithms are faster, but the solution is unstable and noise-sensitive. Problems with training methods are the difficult interpretation of the estimated function f and the choice of the model. Moreover, neural network are difficult to train for high dimensional data [4, Chapter 11].

The results presented in this paper followed from previous research on hyperspectral image inversion [5]. Support Vectors Machines (SVM) are proposed to estimate the functional f . SVM are a training approaches which are robust to the dimensionality and have good generalization abilities [4, Chapter 12]. It has shown good behavior with hyperspectral data for the purpose of classification [6]. Using the *kernel trick*, the estimation of non-linear function f is possible. But, as with neural network, the choice of the kernel function is not straightforward. In this article, several kernel functions were investigated, from linear to non-linear, leading to different levels of accuracy. For linear SVM, connection with a dimension reduction technique, the Gaussian Regularized Sliced Inverse Regression (GRSIR) [5], is discussed. The SVM are compared with GRSIR and Partial Least Square regression in terms of accuracy and computing time.

The SVM and the different kernels are presented in Section 2. Experimental results are reported in Section 3 and discussed in Section 4.

2 Support Vectors Machines Regression

2.1 Regression Problem

The Support Vector Machines are a supervised method for regression or estimation stemming from the machine learning theory. For inversion problems the algorithm, which is called the ϵ -SVR, approximates the functional $f : \mathbf{y} = f(\mathbf{x})$ using solution of the form $f(\mathbf{x}) = \sum_{i=1}^n \alpha_i k(\mathbf{x}, \mathbf{x}_i) + b$, where \mathbf{x}_i are samples from the training set, k is a kernel function and $((\alpha_i)_{i=1, \dots, n}, b)$ are the parameters of f which are found during the training process. The kernel k is used to produce non-linear function. Given a training set, $(\mathbf{x}_i, \mathbf{y}_i)_{i=1, \dots, n} \in \mathbb{R}^d \times \mathbb{R}$, the training

of an ϵ -SVR entails the following optimization problem:

$$\min \left[\frac{1}{n} \sum_{i=1}^n l(f(\mathbf{x}_i), \mathbf{y}_i) + \lambda \|f\|^2 \right] \text{ with } l(f(\mathbf{x}), \mathbf{y}) = \begin{cases} 0 & \text{if } |f(\mathbf{x}) - \mathbf{y}| \leq \epsilon \\ |f(\mathbf{x}) - \mathbf{y}| - \epsilon & \text{otherwise.} \end{cases}$$

The ϵ -SVR satisfies the sparsity constraint: Only some α_i are non-null which corresponding sample \mathbf{x}_i are termed “*Support Vectors*” (SVs). Some limitations come from the learning step: With a large training set, the processing time can be very long. Moreover, the problem is exacerbated when several optimizations for parameter selection are considered.

2.2 Kernel function

The choice of the kernel function is a crucial step with SVM. A kernel function is a similarity measure between two samples and corresponds to a dot product in some feature space. To be an acceptable kernel, the function should be positive semi-definite [4, Chapter 12]. In this work, several kernels were investigated ($\langle \cdot, \cdot \rangle$ in the dot product is \mathbb{R}^d):

- The linear kernel $k(\mathbf{x}, \mathbf{z}) = \langle \mathbf{x}, \mathbf{z} \rangle$.
- The homogeneous polynomial kernel $k(\mathbf{x}, \mathbf{z}) = \langle \mathbf{x}, \mathbf{z} \rangle^p$ and the inhomogeneous polynomial kernel $k(\mathbf{x}, \mathbf{z}) = (\langle \mathbf{x}, \mathbf{z} \rangle + q)^p$, where $q > 0$ is a weight of each degree: $(\langle \mathbf{x}, \mathbf{z} \rangle + q)^p = \sum_{k=0}^p \binom{p}{k} \langle \mathbf{x}, \mathbf{z} \rangle^{p-k} q^k$.
- The Gaussian kernel $k(\mathbf{x}, \mathbf{z}) = \exp(-\gamma \|\mathbf{x} - \mathbf{z}\|^2)$.
- The Spectral kernel $k(\mathbf{x}, \mathbf{z}) = \exp(-\gamma \alpha(\mathbf{x}, \mathbf{z})^2)$, $\alpha(\mathbf{x}, \mathbf{z}) = \arccos\left(\frac{\langle \mathbf{x}, \mathbf{z} \rangle}{\|\mathbf{x}\| \|\mathbf{z}\|}\right)$.

The spectral kernel was first introduced in hyperspectral imagery for the purpose of classification [7]. It is based on the angle between two spectra. It is a scale invariant kernel which is used in k - nn approach or spectral unmixing.

Before running the algorithm, some hyperparameters need to be fitted: *a*) ϵ : which controls the resolution of the estimation. Large values produce rough approximation while small values produce fine estimation. It can be set using some *a priori* on the noise. *b*) λ : Which controls the smoothness of the solution. Large values imply nearly linear function. *c*) Kernel parameters: γ for the Gaussian kernel. Cross-validation is used in this work to select the optimal parameters.

3 Experiments

3.1 Data-set

In this paper, real and simulated data-sets are used. Real data have been collected during orbit 103 by the French imaging spectrometer OMEGA on board Mars Express Mission. A detailed analysis of this image by an expert led to a surface reflectance model. This model allows the generation of many synthetic spectra with the corresponding parameters: The proportions of CO₂, water and dust; and the grain sizes of water and CO₂. Zero-mean multiGaussian noise has

Parameter	GRSIR	PLS	SVM						
			lin.	Gauss.	Spect.	0-Pol	0.5-Pol	1-Pol	2-Pol
Prop. of H ₂ O	0.28	0.32	0.31	0.14	0.25	0.24	0.17	0.14	0.13
Prop. of CO ₂	0.19	0.31	0.30	0.15	0.27	0.27	0.18	0.16	0.15
Prop. of dust	0.11	0.22	0.22	0.09	0.19	0.19	0.11	0.10	0.10
Grain size of H ₂ O	0.34	0.39	0.39	0.15	0.34	0.33	0.23	0.19	0.18
Grain size of CO ₂	0.16	0.24	0.25	0.11	0.21	0.20	0.14	0.12	0.11
CPU time (s)	0.16	0.66	3.57	10.30	5.89	5.98	10.20	60.30	478

Table 1: NRMSE and computing time for GRSIR, PLS and SVM with various kernels. “ x -Pol” means the kernel used was the polynomial kernel with $q = x$. The power of the polynomial kernel was fixed to 9 for each parameter, after cross-validation. The last line of the table corresponds to the training time of parameter “*Prop. of H₂O*” after the selection of optimal hyperparameters.

been added for which the covariance matrix was determined experimentally from the real image. For the validation, separate training and testing data-set has been generated. The notations are as follows: n (respectively n_t) is the number of spectra from the training data (respectively test data), $\mathbf{x}_i \in \mathbb{R}^d, i \in 1, \dots, n$ the spectra from the training data and $\mathbf{y}_i(p) \in \mathbb{R}, i \in 1, \dots, n$ one of the 5 associated parameters (respectively $\mathbf{x}_j^t, \mathbf{y}_j^t, j \in 1, \dots, n_t$). In these experiments, $n = 3584, n_t = 3528$ and the number of spectral bands is $d = 184$. Each parameter $p = 1, \dots, 5$ admits a finite number of values $\mathbf{y}(p)$ regularly distributed in a given interval of variation. The different realization of vector \mathbf{y}_i are generated by building all possible combinations of the individual component values. In the following, the index p is omitted in \mathbf{y} and in its associated f : $f_p(\mathbf{x}) = \mathbf{y}(p)$ is written $f(\mathbf{x}) = \mathbf{y}$.

3.2 Results

The quality of the estimation is assessed by computing the Normalized Root Mean Square Errors (NRMSE):

$$\text{NRMSE} = \sqrt{\frac{\sum_{i=1}^{n_t} (\hat{\mathbf{y}}_i - \mathbf{y}_i)^2}{\sum_{i=1}^{n_t} (\mathbf{y}_i - \bar{\mathbf{y}})^2}} \text{ with } \bar{\mathbf{y}} = \frac{1}{n_t} \sum_{i=1}^{n_t} \mathbf{y}_i \quad (1)$$

where \mathbf{y}_i is the real value and $\hat{\mathbf{y}}_i$ the estimated one. It is close to zero when the predicted values are accurate and becomes larger when predictions are poor.

The SVM regression is compared with GRSIR and PLS, which both first reduce the dimension of the data using \mathbf{x} and \mathbf{y} , and then perform the estimation in the reduced space. PLS is a linear estimator while GRSIR is a piecewise linear estimator, for details see [8]. All the three methods are “*Training Approaches*”.

From Table 1, it is clear that the worst results in terms of accuracy are obtained with linear algorithms: PLS and SVM with linear kernel. Best accuracy are obtained with SVM-Gaussian kernel, followed by SVM-inhomogeneous polynomial kernels with $q \geq 1$. However, the last ones require more time to be trained. SVM with Spectral or homogeneous polynomial kernel yield the lowest accuracy. Considering the training time, SVM lead to longer processing time, for every kernels.

Using the functional f estimated with the simulated training set, inversion are done on the real image. Results are given in Fig. 1, for GRSIR and SVM-

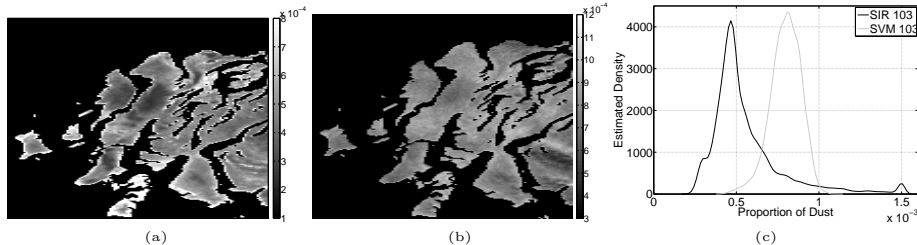


Fig. 1: Proportion of dust estimated by (a) GRSIR, (b) SVM from the hyperspectral image observed from orbit 103 and (c) is the histogram of (a) and (b). Background pixels in black correspond to pixels for which the model used to generated the training sample is not valid and are not considered in (c).

Gaussian kernel. The histogram of the estimated values is also reported and shows a shift between GRSIR and SVM estimates (astrophysical interpretations are given in [9]). However, since no ground data is available, the accuracy of inversion of real image is difficult to appreciate.

4 Discussion

With SVM, the training quality can be assessed by looking at the Support Vectors (SVs) after the training. Selection of many SVs may signify that the optimization problem is hard (but not necessarily badly solved). Fig. 2.(a) shows the fraction of \mathbf{y} corresponding to SVs (light gray) from the training set (dark gray). The fraction increases as \mathbf{y} increases too. To understand why the problem becomes harder, the spectral variance of the simulated spectra as a function of the wavelength is reported in Fig. 2.(b). It is computed as the trace of the covariance matrix of sample \mathbf{x} for which \mathbf{y} is constant. It can be seen that a high \mathbf{y} value leads to: on the one hand a small variance of the simulated spectra, see Fig. 2.(b), and, on the other, a high number of SVs, see Fig. 2.(a). This phenomena is explained by the properties of the physical model: For some values, the model saturates. It implies that when the saturation is reached, increasing the values of the parameter has a little consequences on the simulated spectra (and the variance remains low) thus making the estimation more difficult, due to strong non-linearity between \mathbf{x} and \mathbf{y} . Main practical implication is in the generation of the training samples: Looking at the SVs after a first training provides information to possibly generate new samples for which the estimation is difficult. Finally, note that SVM but other training methods face difficulties in estimating f when saturation is reached.

Contrary to statistical methods such as GRSIR, interpretation of SVM's functional estimation is not possible, excepted for the linear kernel: $f(\mathbf{x}) = \sum_i^n \alpha_i \langle \mathbf{x}, \mathbf{x}_i \rangle + b = \langle \mathbf{x}, \sum_i^n \alpha_i \mathbf{x}_i \rangle + b = \langle \mathbf{x}, \mathbf{w} \rangle + b$. Surprisingly, the vector \mathbf{w} is akin to the vector β estimated with GRSIR [5], see Fig.2.(c). In GRSIR, β is used to reduce the dimension and the estimation f' is done in the reduced space: $f(\mathbf{x}) = f'(\langle \mathbf{x}, \beta \rangle)$. It explains why GRSIR performs better than linear SVM: The estimation is done in the one-dimensional space spanned by β (respectively \mathbf{w})

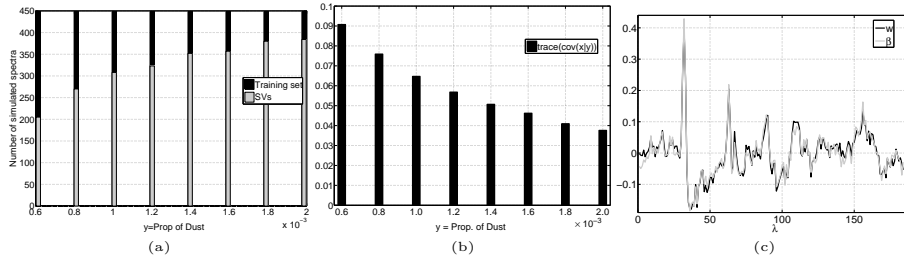


Fig. 2: (a) Fraction of \mathbf{y} (light gray) corresponding to SVs from the training set (dark gray), \mathbf{y} was “Prop. of dust”; (b) Spectral variance of simulated \mathbf{x} as function of \mathbf{y} , $\mathbf{y}(p)$ was “Prop. of dust” ; (c) GRSIR axis β and SVM normal vector \mathbf{w} as function of the wavelength λ .

with a piecewise linear estimator (respectively linear estimator). The precise theoretical comparison is omitted here for the sake of conciseness.

As a conclusion of this work, SVM with non-linear kernel produce accurate results for the inversion of hyperspectral images. Experiments on real data images confirm their robustness to the training set and to the high dimensionality of the data. However, the training time can be dramatically increased for some kernel, making the use of SVM practical situation sensitive. Current research are now oriented in the definition of kernel that handle more efficiently the saturation in the physical model.

References

- [1] S. Douté, B. Schmitt, R. M. C. Lopes-Gautier, R. W. Carlson, L. Soderblom, and J. Shirley. Mapping SO₂ frost on Io by the modeling of NIMS hyperspectral images. *Icarus*, 149:107–132, 2001.
- [2] R. W. Carlson, P. R. Weissman, W. D. Smythe, J. C. Mahoney, the NIMS Science, and Engineering Teams. Near infrared spectrometer experiment on Galileo. *Space Science Reviews*, 60:457–502, 1992.
- [3] D.S. Kimes, Y. Knyazikhin, J.L. Privette, A.A. Abuegasim, and F. Gao. Inversion methods for physically-based models. *Remote Sensing Reviews*, 18:381–439, 2000.
- [4] T. Hastie, R. Tibshirani, and J. Friedman. *The Elements of Statistical Learning: Data Mining, Inference, and Prediction*. Springer, 2003.
- [5] C. Bernard-Michel, S. Douté, L. Gardes, and S. Girard. Inverting hyperspectral images with gaussian regularized sliced inverse regression. In *European Symposium on Artificial Neural Networks, Advances in Computational Intelligence and Learning*, 2008.
- [6] A. Plaza, J. A. Benediktsson, J. Boardman, J. Brazile, L. Bruzzone, G. Camps-Valls, J. Chanussot, M. Fauvel, P. Gamba, A. Gualtieri, J. C. Tilton, and G. Triani. Recent advances in techniques for hyperspectral image processing. *Remote Sensing Environment*, To appear, 2008.
- [7] M. Fauvel, J. Chanussot, and J. A. Benediktsson. Evaluation of kernels for multiclass classification of hyperspectral remote sensing data. In *IEEE International Conference on Acoustics, Speech and Signal Processing. ICASSP’06. Proceedings*, May 2006.
- [8] C. Bernard-Michel, L. Gardes, and S. Girard. Gaussian regularized sliced inverse regression. *Statistics and Computing*, To appear, 2008.
- [9] C. Bernard-Michel, S. Douté, M. Fauvel, L. Gardes, and S. Girard. Retrieval of mars surface physical properties from omega hyperspectral images using regularized sliced inverse regression. *Journal of Geophysical Research*, Submitted, 2008.